Internal Streamline Flow Analysis for Turbopump Inducers under Cavitating and Noncavitating Conditions

R. E. DAVIS* AND L. L. COONS†
Pratt and Whitney Aircraft, West Palm Beach, Fla.
AND
D. D. SCHEER‡
NASA Lewis Research Center, Cleveland, Ohio

This paper discusses the formulation of a hydrodynamic internal streamline flow analysis program which predicts internal flow conditions, including blade pressure loadings, under both cavitating and noncavitating conditions. The analytical model includes the analysis of the size and shape of a distinct three-dimensional vapor cavity on the blade trailing surface. Demonstration of computer program capabilities and correlation of predicted and measured blade loadings are given.

Introduction

INDUCERS typically have been utilized as the initial pump stage in rocket engine propellant feed systems in order to achieve the over-all vehicle weight advantages associated with pump operation at high-speed and low-inlet pressure. A typical inducer is shown in Fig. 1.

There has been no known single hydrodynamic loading model which could adequately predict loads on both the blade leading edge and the channel region of the inducer. Loads are usually determined by applying the two-dimensional, free-streamline-wake model of Stripling and Acosta[1] in the leading-edge region and a two dimensional, axisymmetric model for no-loss, noncavitating flow in the channel region. Total pressure load was then estimated from the results of these two separate approaches. Analytically, this approach was not adequate because it ignored the viscous effects of real fluids and the three-dimensional flow in typical inducers.

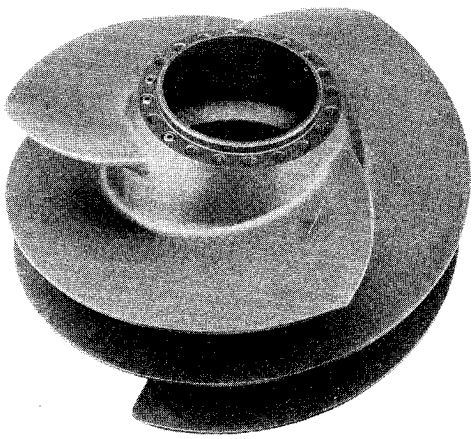

Fig. 1 Typical inducer.

The methods for stress and vibration analyses were also inadequate for inducer blade structural design. The shortcomings in the total structural design area were well recognized by the personnel responsible for inducer design. For the most part, structural integrity was achieved by making proper allowance for the deficiencies in the design methods. In some cases, however, inducer blade failures did occur, and in others it was conceded that the design had been compromised in terms of weight and hydrodynamic performance. It became clear then that technology effort was necessary if high-performance inducers, which were optimum from the standpoints of hydrodynamic and structural performance, were to be achieved. As a result, effort was initiated by the NASA-Lewis Research Center (Contract NAS3-11216) to develop the anlytical models necessary for predicting inducer blade steady-state hydrodynamic pressure loading under cavitating and noncavitating conditions, steady-state stress magnitude and distribution, and blade natural frequencies and relative stresses at resonance. The results of the effort accomplished in the areas of stress and natural frequency predictions are presented in Ref. 2. This paper discusses a computer program which uses an internal streamline flow model for predicting inducer internal flow conditions, including blade pressure loading, under both cavitating and noncavitating conditions. Included are comparisons of predicted and measured blade pressure loadings.

Description of the Computer Program

Under NASA Lewis Research Center Contract (NAS3-11216), a computer program was formulated, developed and evaluated for the prediction of static pressures on the surfaces of inducer blades during cavitating and noncavitating operation. A complete description of the program, including formulation of analytical models and engineering equations, is presented in Ref. 3. A brief description of the models used in the formulation of the computer program is presented in the following discussion.

A. Description of the Computer Program

The basic flow analysis uses a mean streamline, two-dimensional, axisymmetric flow model. It is assumed that the average flow conditions in the blade-to-blade space can

Presented as Paper 70-629 at the AIAA 6th Propulsion Joint Specialist Conference, San Diego, Calif., June 15–19; received July 16, 1970; revision received September 27, 1971. The authors wish to thank NASA Lewis Research Center and Pratt & Whitney Aircraft for permission to publish this paper. The work was conducted under the direction of W. E. Young. J. M. Reddecliff conducted the blade pressure tests. The authors also express appreciation to J. E. Smith and D. R. Edmonds of the Pratt & Whitney Aircraft Computing Group for their contributions in the development of the computer program.

Index category: Hydrodynamics.

* Senior Design Project Engineer.

† Senior Design Engineer.

‡ Project Manager.

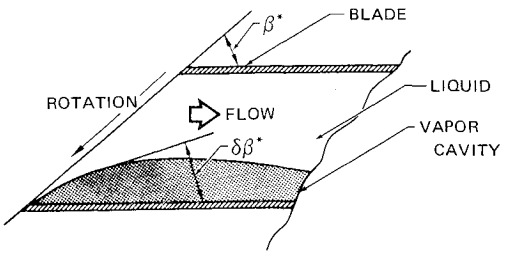

Fig. 2 Distinct vapor cavity.

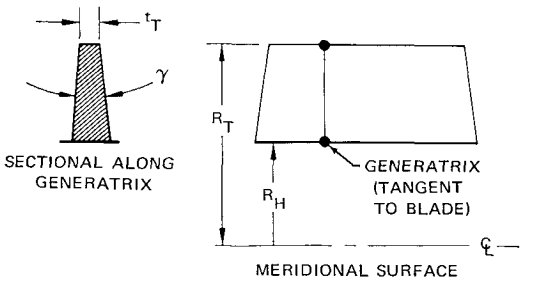

Fig. 3 Thickness distribution of typical blade.

be represented on a meridional surface, so that only a two-dimensional, streamline balancing analysis to satisfy radial equilibrium is required to establish mean velocities, pressures, and flow angles for several radial locations at specified axial stations. A vapor cavity is assumed to exist at all times over some finite distance along the blade suction surface at the inducer inlet, similar to the model of Ref. 1. This cavity, together with the blade, forms a channel for each streamtube that is bounded by two meridional streamlines. It is assumed that all the vapor is contained in the cavity and that the liquid flows in the bounded channel (Fig. 2). This concept is based on the tendency of the liquid to be separated from the vapor due to centrifugal forces arising from curvature of the flow in the blade-to-blade space. Because the vapor merely displaces the liquid in the present flow model, it is considered that the actual blade can be replaced by a pseudo-blade consisting of the real blade plus the cavity. The blade angle is replaced by the mean angle of the pseudo-blade; i.e., the average of the real blade angle and the angle of the surface of discontinuity between the vapor and the liquid measured from the same reference plane. This then produces a local flow "deviation" caused by cavitation, which will add to other deviation effects. These additional effects include leading edge incidence and trailing edge unloading due to circulation around the blades.

Viscous effects are also incorporated in the flow model. A boundary layer analysis determines the amount of flow blockage and momentum defect due to diffusion and to viscous shear forces at the blade surfaces and on the hub and shroud walls. The boundary layer blockage causes the meridional velocity to increase and reduces the work capability of the inducer. The momentum defect causes the mass-average total pressure to be reduced. Thus, the viscosity of the fluid affects both the head input and head output. The presence of a boundary layer and its effect on the cavity formation are also accounted for in the cavity model.

B. Formulation of Analytical Models

Geometric relations

It is assumed that one surface of the inducer blade is generated by a straight line (generatrix) passing through the hub and tip radii. The other surface is assumed to be generated by a straight line inclined at some angle (γ—the taper angle) and displaced some thickness (the blade thickness) with respect to the other generatrix (Fig. 3). To allow for nonradial element blading, it is assumed that the product of radius (R) and the tangent of the blade angle (β^*) varies linearly between the values for the hub and tip. Thus

$$R\tan\beta^* = R_T\tan\beta_T^* - (R_T - R)/(R_T - R_H)[R_T\tan\beta_T^* - R_H\tan\beta_H^*]$$

from which the local value of β^* can be found for any value of R.

The local blade thickness may be obtained from the given tip thickness and the taper angle γ (a small angle)

$$t = t_T + \gamma(R_T - R)$$

The circumferential distance between surfaces of adjacent blades is

$$\tau = 2\pi R/N_b - t/\sin\beta^*$$

where N_b is the number of blades. Although the flow in an inducer is primarily axial, the hub or tip often has a varying radius. The streamlines then may be forced to change radius and, because of the inducer rotation about its axis, Coriolis forces will cause blade pressure loading. The meridional angle of a streamtube (Fig. 4) between two stations is found by dividing the radial displacement by the axial displacement

$$\psi = \tan^{-1}\Delta R/\Delta Z$$

Channel flow relations

The velocity diagram for the mean channel flow at any point is shown in Fig. 4. The governing equations are

$$W = VM/\sin\beta \qquad WU = W\cos\beta \qquad VU = U - WU$$

$$\alpha = \arctan(VM/VU) \qquad V = VM/\sin\alpha$$

$$\beta = \beta^* - \text{deviation}$$

The meridional velocity (VM) is found from the streamtube volumetric flow rate and the flow area normal to the flow direction.

$$VM = Q/A \qquad A = \tau_l(\Delta Y)\cos\psi$$

τ_l is that portion of the blade-to-blade space occupied by the liquid, and ΔY is the radial distance between streamlines (see Fig. 4). The value of τ_l is found by adjusting the geometric blade spacing by the boundary-layer displacement thickness (δ^*) and the cavity height (B), measured circumferentially.

$$\tau_l = \tau - \delta^*/\sin\beta^* - B$$

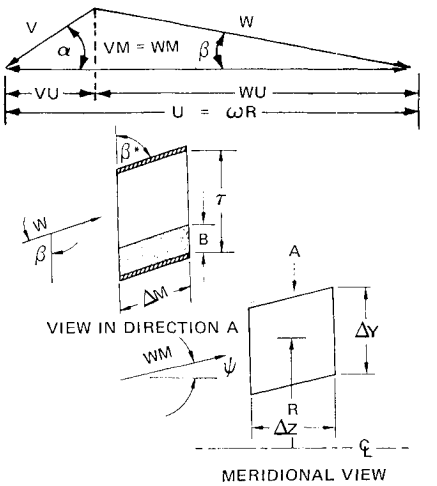

Fig. 4 Illustration of channel element and velocity and angle relations.

If there is no cavity ($B = 0$), the total displacement thickness for both blade surfaces ($2\delta^*$) is used, and the equation becomes:

$$\tau_t = \tau - 2\delta^*/\sin\beta^*$$

Boundary layer blockage on the hub and shroud is accounted for by adjusting the hub and shroud streamtube heights by the local displacement thickness.

$$\Delta Y = \Delta Y - \delta^*/\cos\psi$$

Cavity model

Solutions for inviscid, two-dimensional, free streamline-wake models are found in the literature.[1,4] These predict vapor cavity growth as a function of inducer inlet geometry and operating conditions. Although these idealized models lend much insight into the effects of blading geometry and flow conditions on vapor cavity growth, they do not include real effects resulting from viscous, three-dimensional flow. Viscous effects influence cavity growth through boundary-layer blockage and drag forces. Three-dimensional flow effects result from centrifugal forces, streamline relocation and changes in passage width and height. In the present model, provisions have been made for these additional effects.

In Ref. 1, it was pointed out that the maximum height of the two-dimensional cavity could be calculated from consideration of one-dimensional conservation of mass and momentum parallel to the blades. This suggestion has been developed further in the present model. The same solution for cavity height based on momentum considerations is possible everywhere if the mean flow angle (β) is related to the slope of the surface between the liquid and the vapor, $\delta\beta^*$ (Fig. 2). It is assumed that the "effective" angle of the channel is the average of the angles on the pressure and suction surfaces of the pseudo-blade, i.e.,

$$\beta^* \text{ eff} = \tfrac{1}{2}(\beta^*) + \tfrac{1}{2}(\beta^* - \delta\beta^*) \text{ or}$$
$$\beta^* \text{ eff} = \beta^* - \delta\beta^*/2$$

This assumption makes it possible to calculate the development of the cavity through finite integration techniques so that real fluid effects can be included.

The finite cavity is generated so that conservation of momentum parallel to the blades is satisfied at all times. Interdependence between the cavity shape and the streamline location requires an iterative procedure for solution of the flow field. The forces involved in the momentum balance include normal surface forces, shear surface forces, and a body force due to centrifugal effects. Figure 5 shows the basic fluid element used in the calculation of the change in cavity height between two axial stations. Figure 6 defines the surfaces and dimensions used in calculating the forces acting on the fluid element.

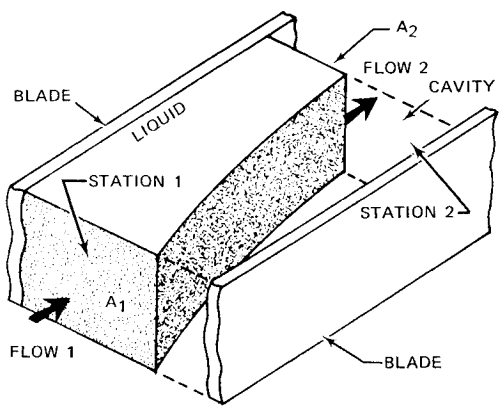

Fig. 5 Fluid element with vapor cavity.

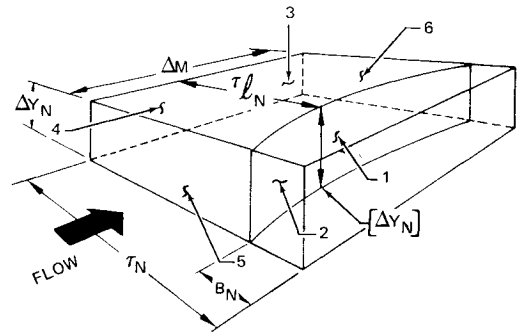

Fig. 6 Surface of fluid element on which forces act.

Surface 1 defines the boundary between the cavity and the liquid. Surfaces 2 and 3 are the streamtube interfaces between the lower and upper streamtubes with the exception of special cases where the hub or tip streamtube is being analyzed. Surface 4 is the blade/liquid interface. Surfaces 5 and 6 are the inlet and exit flow areas of the streamtube element.

The complete formulation of all forces is lengthy and will not be given here. (See Ref. 3 for a detailed derivation.) Basically, pressure forces parallel to the blades will exist on surfaces 1, 5, and 6 (Fig. 6). If the streamtube height (ΔY_N) changes between stations, there will be additional components of pressure forces parallel to the blades on surfaces 2 and 3. If the geometric spacing between blades (τ_N) changes, there will be a contributing pressure force on surface 4. Significant shear forces will exist on surface 4 for all streamtubes and on surfaces 2 and 3 for the hub and shroud streamtubes, respectively. The shear forces on the surfaces between streamtubes are assumed to be small compared with the other forces.

A body force will exist wherever the streamtube is inclined with respect to the axis of rotation in the meridional plane (Fig. 7). This force is the component in the streamline direction resulting from the centrifugal force in the radial direction.

$$F_C = F_R \sin\psi$$

The total force acting on the fluid element is equated to the change in momentum of the fluid parallel to the blades between two stations

$$F_T = \rho Q[W_2 \cos\delta_2 - W_1 \cos\delta_1]$$

where δ_1 and δ_2 are the local deviation angles and ρ is density. Adjustments are made to the cavity slope ($\delta\beta^*$) and height (B) at each station such that the above expression is satisfied. This procedure is repeated for each streamtube at successive stations, while satisfying radial equilibrium, resulting in the definition of a three-dimensional cavity shape. For each streamtube, the cavity is allowed to grow until its slope becomes approximately zero (parallel to the blades). Then,

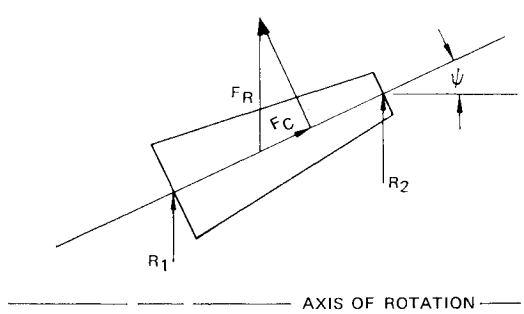

Fig. 7 Element centrifugal force.

it is assumed that the cavity collapses in a turbulent wake. This causes a sudden expansion of the liquid flow and results in a loss of total pressure as well as a rise in static pressure. These values are found by specifying a rate of collapse (i.e., wake mixing) and solving for static and total pressure from the equations for continuity of mass and momentum.

The cavity collapse is defined by a decrease in cavity height (normal to the blade) which is linear with respect to distance along the blade. This model is based on the mixing of a freejet boundary. Empirical data[8] indicates that the linear rate of growth of half the width of the jet mixing zone (and therefore, the reduction of cavity height in this case) corresponds to an angle of approximately 2.8° with respect to the blade surface.

Deviation of the flow

It is assumed that the flow will tend to follow the mean direction of the passage formed by the blades (or by the pseudo-blades under cavitating conditions). Because of leading edge incidence and circulation, however, the flow is not parallel to the blades at the blade leading and trailing edges. Fluid inertia prevents discontinuous changes in the flow direction. Therefore, relations for the distribution of deviation angle in terms of inlet and exit boundary values must be established. These relations have been derived from two-dimensional potential flow analyses and empirical correlation.[3]

A step change in the blade angle (β^*) results in an asymptotic change in the flow angle (β). For example, at the inducer inlet the flow approaches at some incidence angle (δ_0). As the flow enters the channel between blades, the deviation (δ) between blade angle and flow angle will approach zero. Solution by two-dimensional potential flow analysis[3] gives a variation in inlet deviation dependent upon the distance-to-gap ratio. The effect of this inertial lag on the deviation due to incidence is illustrated in Fig. 8. It is noted that the deviation due to incidence is removed in a distance of approximately one gap. If the blade angle varies in the flow direction, the deviation at each station can be found by treating X as the distance between stations and δ_0 as the value of deviation at the previous station.

The value of the deviation angle at the inducer blade trailing edge (δ_e) is found by using an empirical deviation formula similar to Carter's rule; i.e., for a given blade geometry the exit deviation is proportional to a flow turning angle. In the present model, this is the angle the flow would experience if the flow were parallel to the blade at the exit, i.e.

$$\delta_e/(\beta_e^* - \beta_0) = \text{const}$$

where β_e^* is the blade exit angle and β_0 is the fluid inlet angle. The constant is assumed to be a function of blade solidity (σ, or chord/gap ratio) as normally defined by Carter's rule

$$\delta_e/(\beta_e^* - \beta_0) = C_e\sigma^{-1/2}$$

The value of the constant, C_e, has been determined for the present model by varying it until the noncavitating ideal head rise predicted for the inducer in[5] agreed with the measured data over the operating flow range. The value thus determined is 0.28, which is consistent with the magnitude from previous empirical correlations for cascades with high-stagger angles.[6,7] Upstream of the trailing edge, the deviation due to trailing-edge unloading (or circulation) is assumed to approach the exit value exponentially, similar to the distribution of deviation due to leading edge incidence given earlier (Fig. 8).

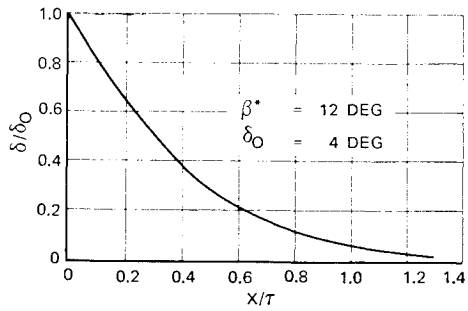

Fig. 8 Illustration of inertial effect on deviation due to incidence.

Viscous effects

A two-dimensional, turbulent, incompressible boundary layer model, including the effect of pressure gradients, is used for calculation of the viscous flow effects on inducer operation. A finite difference solution of the von Kármán momentum integral equation and Garner's shape factor equation[8] is used for each streamtube. The skin-friction coefficient is found from the equation of Ludwieg-Tillman. It is assumed that since there is very little secondary flow in the inducer, migration of the boundary layer in a direction transverse to the flow direction is not significant.

Mid-channel relative velocity gradients are used in the boundary layer equations. The underlying assumption is that the boundary layer characteristics thus obtained are representative of the average characteristics for the pressure and suction surfaces of the blades. Similarly, these values are average for the hub and shroud end wall boundary layers. Pressure losses are calculated from the momentum defect in the boundary layers, and flow blockage is found from the calculated displacement thickness. The skin-friction coefficient is used to calculate the wall shear force used in the cavity model.

Radial equilibrium

Solution of the flowfield in the meridional plane requires that conservation of radial momentum be satisfied at all axial stations. In the present model, the calculated radial pressure gradient includes the effects of streamline curvature and radial acceleration as well as the effect of tangential swirl velocity (VU) used in simple radial equilibrium. Although inducer flow is primarily axial, the pressure gradient caused by streamline curvature can become significant relative to that caused by swirl, particularly during cavitating operation when the streamlines shift radially as the cavity develops. The total radial gradient of static pressure is given by

$$1/\rho dp/dR = VU^2/R - VM^2\cos^2\psi d\psi/dZ - VM\sin\psi\cos\psi dVM/dZ$$

The calculated pressure gradient on a streamline is compared with the finite difference pressure gradient calculated between the streamtubes on each side of the streamline. The radial locations of all interior streamlines then are varied iteratively by relaxation technique to minimize the error in satisfying radial equilbrium.

Inlet and exit calculations

Special calculations are included for stations upstream of the inlet and downstream of the exit of the inducer blade. Radially varying flow conditions at the inlet can be specified. The exit calculations, which are based on simple radial equilibrium considerations, include the effects on velocities from mixing out the blade trailing-edge wake caused by boundary layer and blade trailing-edge thickness. The "apparent" exit deviation is affected by these changes in velocities. Overall performance parameters, such as ideal and actual headrise and efficiency, are calculated for each streamtube and are mass-flow-averaged for inducer performance.

Blade pressure loading

A special routine is included in the program for calculating the blade surface static pressures and pressure differential for input for blade stress calculations.[2] At each axial station, the mid-channel pressure gradient normal to the blade surface is calculated for each streamtube. This gradient is used to extrapolate linearly from mid-channel to the blade surfaces in a normal direction and obtain surface static pressures. Near the leading edge suction surface and the trailing edge pressure surface, the mid-channel static pressure and pressure gradients are calculated based on two-dimensional potential flow theory and the known boundary conditions far upstream and downstream of the inducer and inside the channel region of the blades. After all blade surface static pressures are known, the complete blade pressure loading distribution can be obtained.

Evaluation of the Computer Program Results

Several evaluations of the analytical models incorporated in the computer program have been made. These include comparison of results from the computer program both with exact solutions for simple problems and with inducer test data under cavitating and noncavitating conditions, including over-all performance as well as blade pressure loadings.

A. Comparison of Program Results with Exact Solutions

Preliminary evaluation of the accuracy of portions of the computer program models can be obtained by comparing results with known exact solutions for simple cases. These include the inviscid, noncavitating flow through a rotating wheel with many axial blades (paddlewheel) and the free-streamline-wake model analysis for a plane cascade of thin plates under cavitating conditions.

Paddlewheel flow

The flow was analyzed with the present computer program by specifying zero viscosity and using seven streamtubes. The exact solution for radial distribution of pressures and velocities was found by satisfying simple radial equilibrium. Figure 9 shows the results of the comparison of static pressure variation inside the paddle-wheel. Similarly, good agreement was obtained for other parameters. This comparison validates the basic streamline balance procedures incorporated in the program.

Cavitating cascade analysis

The exact solutions for cavity shapes in a cascade of flat plates, based on the free streamline-wake model, can be found by conformal mapping. The typical results for a 15° cascade

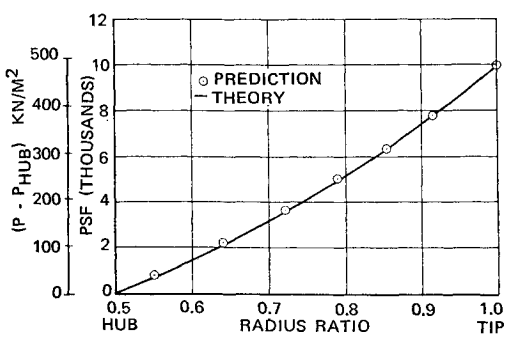

Fig. 9 Paddle wheel test case—radial equilibrium.

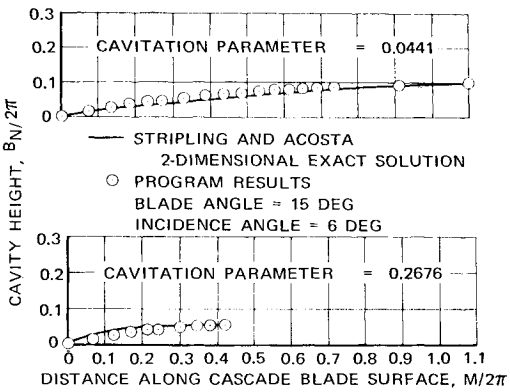

Fig. 10 Comparison of cavity height prediction.

presented in[1] can be used for comparison with results from the present computer program. These were obtained by specifying zero viscosity and defining an inducer with a hub/tip ratio approaching unity and a large number of blades. This provided approximately a plane cascade for inviscid flow analysis. Fig. 10 shows the comparison of computer results with those obtained from the exact solution of[1] for two values of inlet cavitation parameter. The level of agreement shown demonstrates that the three-dimensional, viscous, finite-difference cavity model in the present program can reasonably produce the cavity shape for the special case of inviscid, two-dimensional flow.

It is interesting to compare results of calculating the cavity shape in an actual inducer both by the present program and by the free streamline-wake model. The inducer described by Fig. 15 and Table I was used for this comparison. The operating condition was the same as in Fig. 17. The value of the maximum cavity height normal to the blade and the distance from leading edge to the point of maximum cavity height (Fig. 11) were calculated for varying spanwise locations.

Table 1 Description of test inducer

	Inlet	Exit	
Tip diameter (in.)	7.0	7.0	
Hub diameter (in.)	2.8	3.74	
Blade angle (deg.)			
tip	8.0	10.0	
hub	19.35	18.25	
Blade thickness (in.)			
tip	0.130	0.130	
hub	0.130	0.130	
Rotor speed (rpm)			4900.
Number of blades			3.
Axial length (in.)			3.5

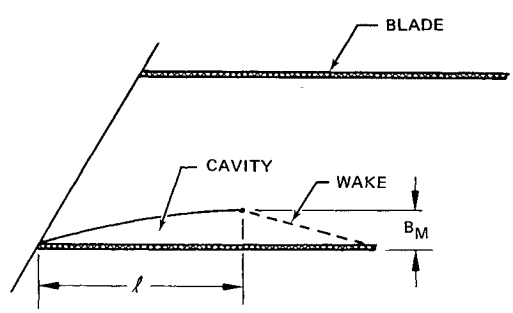

Fig. 11 Vapor cavity dimensions.

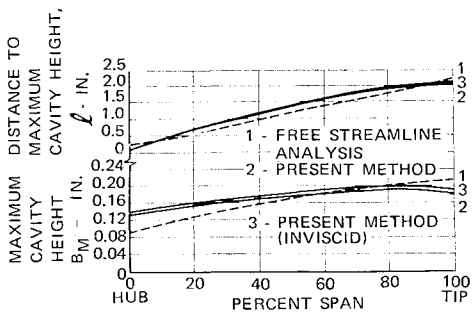

Fig. 12 Comparison of predicted cavity dimensions, free-streamline analysis and present method.

Figure 12 shows the results of the calculations. The present computer program was run both with and without friction to separate viscous and three-dimensional effects. The cavity height as shown is the distance from the pressure surface of the blade.

Apparently, the differences in results between the free streamline-wake model and the present model are caused primarily by streamline convergence. This condition violates the assumption of two-dimensional flow that is incorporated in the free-streamline analysis. The effect of friction, which adds boundary-layer blockage, is a small decrease in cavity height and length. Conceivably, the difference in results might have been even greater if the inducer had a swept leading edge. In that case the streamlines would begin relocating due to blade blockage and fluid swirl occurring at the hub before occurring at the tip. It would be desirable to verify the computer program predictions for the effect of a swept leading edge by testing an inducer with two or three levels of sweepback and comparing test data with program predictions.

B. Comparison of Program Result with Test Data

Additional evaluation of the accuracy and adequacy of the computer program models can be made by comparing results with actual test measurements. These include overall inducer performance as well as blade pressure loadings. Both cavitating and noncavitating operating conditions are used in these comparisons.

Over-All Inducer Performance

As stated earlier, the test data from Ref. 5 were used to determine the constant to be incorporated in the exit deviation model. Figure 13 shows the comparison between program results and test data for the noncavitating actual head rise coefficient (Ψ) and efficiency (η) for the same inducer. Since the calculated ideal head rise has been made the same as the

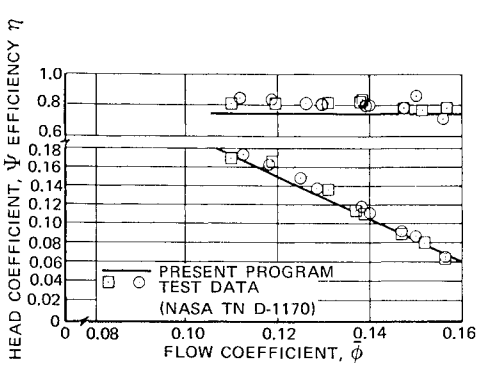

Fig. 13 Noncavitating performance of NASA 12° helical inducer.

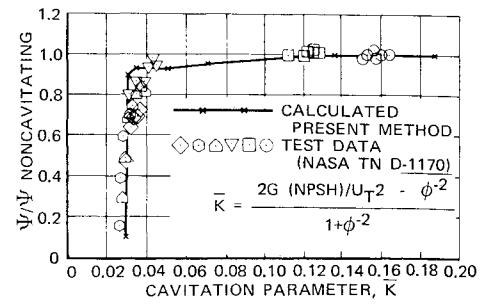

Fig. 14 Cavitating performance of NASA 12° helical inducer.

test data, the differences in actual head rise coefficients and efficiency in Fig. 13 are due to the higher losses calculated by the program. Even at the high level of inlet pressure used in the calculations, a significant vapor cavity height, approximately 15% of the passage, was calculated on the blades at a low-flow coefficient. High losses associated with the dumping of this cavity could account for the differences in Fig. 13.

Figure 14 shows the comparison between the test data and the program results for the cavitating performance of the same inducer. The predicted effect of reducing NPSH is verified by the test results. The predicted value of cavitation parameter (K) at which complete head breakdown occurs agrees closely with the test data.

Blade Surface Pressures

As part of the NASA/P&WA program, an inducer was designed, fabricated and instrumented to obtain blade surface pressures. (A detailed description of the instrumentation arrangement is given in Ref. 3.) The inducer was tested in a research water loop facility, and blade surface pressures were measured at several values of flow rate, rotor speed, and inlet pressures. Pressures were recorded from inlet to exit at two radial locations. Operating points included both cavitating and noncavitating conditions.

The geometry of the test inducer used for input to the computer program is shown in Fig. 15 and Table I. Predictions of blade surface pressures were made for operating conditions

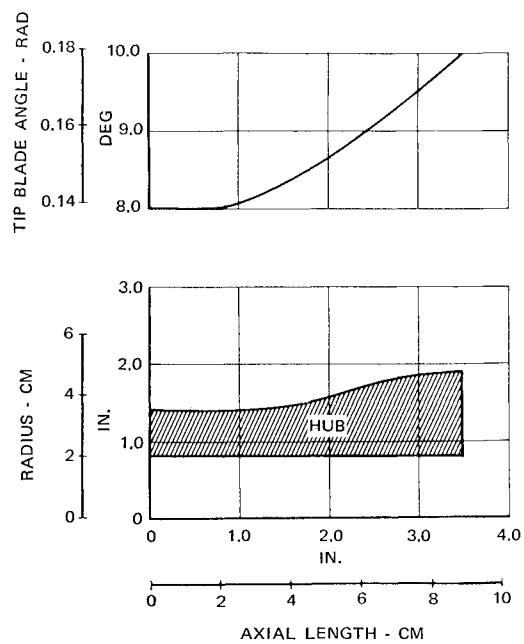

Fig. 15 Task III inducer flow path and blade angle distribution.

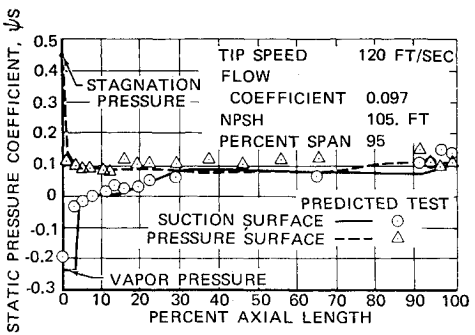

Fig. 16 Comparison of blade surface pressure coefficients at highest NPSH.

for which test data were available.[3] Figures 16 and 17 illustrate typical comparisons between predicted and measured data for one radial location. The pressures have been normalized by using a static pressure coefficient (ψ_s) defined as

$$\psi_s = (P_s - P_{0_1})/\rho U_T^2$$

where U_T = tip speed, P_s = blade static pressure, and P_{0_1} = inducer inlet total pressure.

Figure 16 is for the operating condition that had the least amount of cavitation. The measured data indicate very little, if any, cavitation existing on the suction surface of the blade. The computer program predicts a short cavity on the suction surface. In general, however, the agreement between predicted and measured pressures is reasonable. Figure 17 shows a comparison under cavitating conditions. Although the over-all head rise and efficiency of the inducer had not changed significantly from the noncavitating condition, the measured suction surface pressures near the leading edge indicate the presence of a region of vapor pressure. The computer program predicts a vapor cavity length which is in reasonable agreement with the length of the region of vapor pressure.

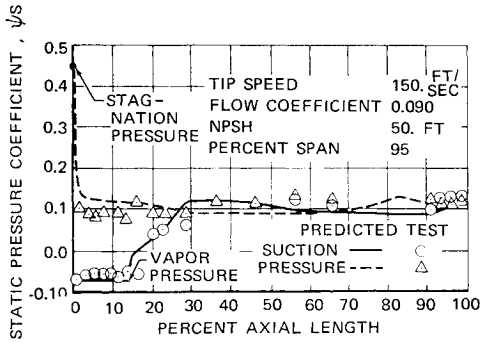

Fig. 17 Comparison of blade surface pressure coefficients at lowest NPSH.

Summary

An analytical inducer internal streamline flow model, which incorporates the anlysis of a distinct three-dimensional vapor cavity, has been formulated and programmed. Comparison of program results with exact solutions of simple problems of both cavitating and noncavitating conditions were successful. Further validation of the analytical models has been made for cavitating and noncavitating operation of inducers. Program results compared favorably with measured over all performance and blade surface pressures. Comparison of cavity dimensions predicted by the present model and an inviscid, two-dimensional, free-streamline model indicates that the effect of streamline convergence or divergence on the cavity shape is significant.

References

[1] Stripling, L. B. and Acosta, A. J., "Cavitation in Turbopumps —Part I," 61-WA-112, Sept. 1962, ASME.

[2] Barten, H. J. and Scheurenbrand, J. A., "Stress and Vibration Analysis of Inducer Blades Using Finite-Element Technique," AIAA Paper 70-630, San Diego, Calif., 1970.

[3] "Study of Inducer Load and Stress," PWA FR-7304, 1970, Pratt & Whitney Aircraft, West Palm Beach, Fla.

[4] Jakobsen, J. R., "Supercavitating Cascade Flow Analysis," 64-FE-11, Feb. 1964, ASME.

[5] Soltis, R. F., Anderson, D.A., and Sandercock, D. M., "Investigation of the Performance of a 78° Flat-Plate Helical Inducer," TN D-1170, March 1962, NASA.

[6] Carter, A. D. S. and Hughes, H. P., "A Theoretical Investigation Into the Effect of Profile Shape on the Performance of Aerofoils in Cascade," R & M 2384, March 1946, British Aeronautical Research Council.

[7] Lieblein, S., "Incidence and Deviation-Angle Correlations for Compressor Cascades," *Journal of Basic Engineering*, Sept. 1960.

[8] Schlicting, H., *Boundary Layer Theory*, McGraw-Hill, New York, 1960.